Bankfull Transport Capacity and the Threshold of Motion in Coarse-Grained Rivers

Article *in* Water Resources Research · December 2019

DOI: 10.1029/2019WR025455

2 authors:

Colin Phillips
Utah State University

Douglas J. Jerolmack
University of Pennsylvania

Bankfull transport capacity and the threshold of motion in coarse-grained rivers

Authors: C. B. Phillips[1] and D. J. Jerolmack[2]

[1]Civil and Environmental Engineering, Northwestern University, Evanston, IL

[2]Earth and Environmental Science, University of Pennsylvania, Philadelphia, PA

Corresponding author: Colin Phillips (colinbphillips@northwestern.edu)

Key points:

- In natural rivers critical Shields stress co-varies with bankfull Shields stress in a manner predicted by theory
- Empirical relations between slope and critical Shields stress are based on a partial sample of the known parameter space for gravel rivers
- Predictions of changes in bankfull transport capacity based on the correlation between slope and the threshold of motion can be spurious

Abstract

The threshold stress for bed sediment transport exerts a primary control on the geometry and stability of coarse-grained rivers (diameter ≥ 5 mm). Understanding how river bed mobility couples to channel form is a key mechanistic link for predicting river response to external perturbations such as land use practices and changing climate. Unfortunately, determination of a representative threshold stress is notoriously difficult in the field. Empirical studies have observed that the critical dimensionless shear (Shields) stress (τ_{*c}) is correlated with channel slope, a property that is substantially easier to estimate. Mechanistic models have been developed to explain the observed correlation; however, limited field data precludes the widespread application of these models. For practical reasons, the empirical regressions between slope and τ_{*c} are utilized as predictive models. Through a large compilation of field data, we demonstrate that there are two significant problems with using the empirical regressions: (1) they are based on a partial sampling of the observed parameter space of coarse-grained rivers; and (2) they do not capture the covariation between the bankfull Shields stress (τ_{*bf}) and τ_{*c}. These regressions provide spurious predictions for the bankfull transport capacity (τ_{*bf}/τ_{*c}) of gravel-bed rivers. When site-specific empirical measurements of τ_{*c} are made, coarse-grained rivers exhibit a remarkably constant transport capacity that is in close agreement with equilibrium-channel theory ($\tau_{*bf}=1.2\tau_{*c}$). From these data we advocate that, in the absence of measurements, τ_{*c} can be reasonably estimated from the τ_{*bf} using equilibrium-channel theory.

1. Introduction

A longstanding interest in the science and engineering of rivers is in understanding which flows are responsible for transporting sediment and how these flows both organize and are shaped by the channels that convey them (Glover & Florey, 1951; Henderson, 1963; Leopold & Maddock, 1953; Leopold & Wolman, 1957; Wolman & Miller, 1960). This understanding is increasingly important if we are to predict a river's response under future landscape and climate scenarios (Hempel, 2018; Phillips et al., 2018; Schmidt & Wilcock, 2008; Slater et al., 2015; Slater & Singer, 2013). River channel stability is, to first order, controlled by the transport threshold of material in the bed or channel banks, whichever is harder to entrain (Dunne & Jerolmack, 2018; Schumm, 1960). In coarse-grained rivers, here considered to be generally gravel-bedded (median diameter, D_{50} ≥ 5 mm), the bed sediment is most often harder to entrain than the banks and hence sets the threshold for altering channel geometry. Single threaded gravel-bed river channel geometry has been analytically linked to bed-load sediment transport through hydraulics (Parker, 1978, 1979): the summary result is that channel geometry is adjusted so that fluid stress is at the threshold of motion at the toe of the river banks, and modestly above threshold in the channel center. This theory has been broadly validated in natural channels and laboratory experiments (Dade & Friend, 1998; Dunne & Jerolmack, 2018; Métivier et al., 2017; Parker et al., 2007; Phillips & Jerolmack, 2016; Pitlick et al., 2013; Pitlick & Cress, 2002; Reitz et al., 2014; Seizilles et al., 2014).

Yet, the threshold of motion in natural channels remains very challenging to accurately measure, and data to evaluate hypotheses remain sparse (Buffington & Montgomery, 1997; King et al., 2004; Mueller et al., 2005) when compared to the available databases of river hydraulic geometry (see Church & Rood, 1983; Li et al., 2014; Trampush et al., 2014). Standard practice is to assess mobility through the use of the Shields curve, which is perhaps most valid under idealized conditions such as normal flow and unimodal bed sediments (Lamb et al., 2008; Shields, 1936; Wiberg & Smith, 1987). However, even in idealized laboratory conditions the threshold of motion varies with particle protrusion, bed texture, grain size distribution, and the structure of the granular bed (Houssais et al., 2015; Kirchner et al., 1990; Masteller & Finnegan, 2017; Pender et al., 2007; Prancevic & Lamb, 2015b; Shvidchenko & Pender, 2000; Wilcock, 1998; Zimmermann et al., 2010). For natural flows where conditions are decidedly less uniform or steady, the threshold of motion is commonly treated as the measurable motion of a surface layer (Parker, 1990) and varies both spatially within a reach, temporally within a flood, from flood to flood, with sediment supply and availability, and with the method of measurement (Buffington & Montgomery, 1997; Johnson, 2016; Lisle et al., 2000; Marquis & Roy, 2012; Masteller et al., 2019; Pfeiffer et al., 2017; Prancevic & Lamb, 2015b; Turowski et al., 2011; Yager et al., 2012, 2018). Within a reach, spatial heterogeneity in grain size organization can result in unequal mobility especially at shear stresses near the threshold, where smaller particles are susceptible to turbulent bursts and bed-load flux measurements may strongly reflect partial transport and not the entire bed (Paola & Seal, 1995; Recking, 2013; Wilcock & McArdell, 1997). These phenomena may be described by some distribution of the threshold for a given reach; however, additional lines of evidence indicate that even this distribution may be nonstationary and may drift through time due to changes in the river bed state (Charru et al., 2004; Houssais et al., 2015; Johnson, 2016; Masteller et al., 2019).

In natural streams and rivers, a large variety of methods and techniques have been used to measure bed-load flux and the threshold of motion. These methods largely fall into two categories, active or passive monitoring. Active methods involve direct measurement of the flux via physical samplers or registering of impacts (for examples see Bunte et al., 2013; Gray et al., 2010; King et al., 2004; Reid et al., 1985; Rickenmann et al., 2012) while passive techniques involve visual determination, tracer particles, competence or largest mobilized particle, acoustics, and seismometers (see Barton, 2006; Hsu et al., 2011; Phillips et al., 2013; Phillips & Jerolmack, 2014; Rickenmann et al., 2012; Roth et al., 2016; Wilcock, 1992). However, these methods remain resource intensive and are not guaranteed to produce a robust estimate of a threshold of motion unless sampled over larger space and timescales (Monsalve et al., 2016; Recking, 2013). In some cases, acquiring sufficient bed-load flux measurements could take years due to the recurrence intervals of floods that are capable of transporting sediment. Despite the threshold's importance, there is currently a lack of low-cost reliable methodologies to rapidly assess this variable in the field.

Natural and laboratory estimates of the threshold of motion have been observed to possess a positive correlation with channel slope (Lamb et al., 2008; Mueller et al., 2005). Though initially counter intuitive, that sediment particles become harder to move at higher gradients, mechanistic grain-scale models incorporating relative roughness, reduced turbulent intensity, partitioning of the total shear stress, particle friction angles, and particle lift and drag forces have explained this correlation under a variety of experimental conditions (Ferguson, 2012; Lamb et al., 2008, 2017a, 2017b; Prancevic et al., 2014; Prancevic & Lamb, 2015a, 2015b; Recking, 2009). Many of the aforementioned processes necessarily covary with slope and relative roughness, however additional experiments have isolated reduced turbulent intensity and the lift force as primary causes for the increase of the threshold of motion with slope (Lamb et al., 2017a). Despite these advances, the difficulty of measuring the threshold of motion in the field, combined with the challenge in measuring the necessary parameters to apply the mechanistic models, has led to an over-reliance on empirical regressions between slope and threshold for natural rivers. In this contribution, we demonstrate that there are two significant problems with using slope-based empirical regressions as they: (1) are based on a partial sampling of the parameter space of bed-load rivers, and cannot be extrapolated outside of that range; and (2) do not capture the observed covariation between the bankfull (τ_{*bf}) and critical (τ_{*c}) Shields stresses and thus can provide spurious predictions of the bankfull transport capacity (τ_{*bf}/τ_{*c}). An important point to note here is that none of the authors of the original studies exploring the correlation between slope and the threshold of motion (Ferguson, 2012; Lamb et al., 2008; Mueller et al., 2005; Recking, 2009) suggested that the empirical regressions be used in a predictive fashion, or in lieu of actual measurements. The use of the empirically based regressions, due to the aforementioned problems, can lead one to conclude that bankfull transport capacity varies among gravel-bed rivers, while direct measurements of the threshold indicate that τ_{*bf}/τ_{*c} is remarkably constant and in quantitative agreement with theoretical predictions (Parker, 1978, 1979). Due to the close match with theory, we suggest that the bankfull Shields stress can be used to estimate the threshold of motion as an alternative to the slope-based regressions. Additionally, we illustrate how using an empirical slope-based regression can lead one to draw potentially incorrect conclusions, through various sampling strategies of the compiled gravel-bed rivers.

2. Data and Methods

Two types of field sites are used within this study: (1) field sites where the threshold of motion can be reliably estimated from bed-load flux estimates (n=68), and (2) a compilation (n=739) of coarse-grained river hydraulic geometry to place the hydraulic geometry of the sites where the threshold of motion was measured into a broader context. For clarity, we refer to the first set as the 'threshold' data and the second as the 'compilation' data throughout the remainder of the manuscript. The compilation and threshold sites both represent samples of the global population of gravel rivers, however the compilation provides a more complete picture of the variability within gravel rivers, while the threshold sites represent a smaller partial sample of the of the compilation's hydraulic geometry parameter space. The majority of the threshold field sites come from the study of Mueller et al. (2005) with additional data compiled from the works of Recking (2010, 2013), King et al. (2004), and others (Andrews, 1994, 2000; Andrews & Erman, 1986; Bunte, 1998; Erwin et al., 2011; Ferguson & Church, 2009; Hinton et al., 2017; Jones & Seitz, 1980; May et al., 2009; May & Pryor, 2013; McLean et al., 1999; Milhous, 1973; Mueller

& Pitlick, 2014; Parker et al., 1982; Phillips & Jerolmack, 2014; Rankl & Smalley, 1992; Ryan et al., 2005; Ryan & Emmett, 2002; Smalley et al., 1994; Whitaker & Potts, 2007; Wilcock et al., 1996). The compilation data represent field measurements at bankfull conditions of slope (S), width (W, m), discharge (Q, m^3/s), depth (H, m), and the median bed surface grain size (D_{50}, m). These data represent the combination of coarse-grained single thread gravel bed rivers compiled by Li et al. (2015), Trampush et al. (2014), Church and Rood (1983), and Phillips and Jerolmack (2016). All of the above parameters are not available for each site as the compilation reflects the state of the data as collected by the original authors with duplicates removed.

2.1 Calculating the Threshold of Motion

For the threshold sites we follow the methodology of Mueller et al. (2005) for determining the threshold of motion. Their thorough compilation and analysis form the core dataset from which the correlations between slope and the threshold of motion have been drawn. We summarize the methodology here as it pertains to understanding the current contribution. The primary data represent measurements and estimates of the reach-scale fluid driving stress (nondimensionalized as the Shields stress, τ_*) and sediment flux per stream width (q_s, kg/m/s). From these data we define the threshold of motion as the dimensionless critical Shields stress (τ_{*c}). The reach and cross section scale Shields stress is estimated using hydraulic geometry variables as:

$$(1) \qquad \tau_* = \frac{\tau}{(\rho_s - \rho) g D_{50}}$$

where τ is the shear stress (Pa), ρ_s is the density of sediment (taken here as 2650 kg/m^3), ρ is the density of water (1000 kg/m^3), and g is the acceleration due to gravity (9.81 m/s^2). We approximate the shear stress via the depth-slope product as $\tau = \rho g h S$, where h is the flow depth. To standardize the measurements across field sites, we nondimensionalize the transport rate as:

$$(2) \qquad W_* = \frac{R g q_s}{\rho_S (\tau/\rho)^{1.5}}$$

where R=1.65 is the submerged specific density of the sediment (see Parker et al., 1982; Parker, 1990). The threshold of motion is determined as the median value of Shields stress at which the dimensionless transport rate intersects a reference transport rate of W_*=0.002 (Parker, 1990; Mueller et al., 2005). The use of a reference transport rate to determine a threshold of motion means that, strictly speaking, we have determined the reference Shields stress (τ_{*r}), which is close but not necessarily equal to τ_{*c}. Throughout the rest of the manuscript references to the threshold of motion and data analysis specifically refer to τ_{*r} as a proxy for τ_{*c}. For field sites where the bulk of the sediment flux measurements are either above or below the reference transport rate, we estimate the point of intersection by fitting a surface-based transport relation $W_*=0.002(\tau/\tau_r)^{14.2}$ (Parker, 1990). All told we have examined sediment transport data for 132 sites and retained 68 of them for the following analysis. Of the 68 sites, one site (the Mameyes River) used tracer particles to estimate the threshold of motion (see Phillips and Jerolmack, 2014). The 64 excluded sites were not retained for a variety of reasons, the most common being missing data, insufficient sample size, and conflicting parameter estimates. In some cases, field sites were excluded if we could not estimate a reliable reference threshold due to the absence of a trend within the flux measurements. This occurs in several channels with large sand fractions and for sites where particles approaching the size of the stream bed D_{50} were never mobilized. Both of these issues result in no relation between Shields stress and flux for the range of stresses reported. For a broader discussion of potential problems with these and similar data see Recking (2010; 2013).

2.2 Estimating the Channel Bankfull Transport Capacity

The bankfull transport capacity (τ_{*bf}/τ_{*r}) is estimated for the threshold data using equation (1) for τ_{*bf}, while τ_{*r} is determined from bed-load flux measurements. In other words, τ_{*bf} is determined from channel morphology, and hence independently from τ_{*r}. In a few cases, our estimates of the variables required to compute τ_{*bf} and τ_{*r} based on the raw data differ from the values reported in the original studies. These differences are generally small, and we use the reported values in deference to the previous authors. We have only used sites that characterize the bankfull depth as a morphologic break between the active channel and a flood plain or non-channelized area (refer to Williams (1978) for additional common metrics of bankfull depth), as expansive flood plains are not always evident in mountain channels. For several field sites with irregular cross sections or large gravel bars we estimated the bankfull depth as the average depth across the active channel, which excludes the banks and large gravel bars from the height estimates. For these sites, the hydraulic radius becomes increasingly skewed by the bar and no longer reasonably approximates the stress imposed on the stream bank adjacent to the flow. Overall this results in a slightly higher estimate of the bankfull depth for some reaches, but matches the hydraulic radius calculations for more uniform or rectangular cross sections. We have excluded field sites where we cannot reliably estimate both τ_{*r} and τ_{*bf}; difficulties in calculating the latter are due to insufficient data to calculate H, S, and the D_{50}. In some cases, we have excluded field sites where there are no raw data available and we are not able to acquire reliable estimates of these parameters from other sources. Additionally, we have excluded several field sites where multiple sources report conflicting estimates of the same hydraulic geometry parameters and we cannot determine which ones are representative of the channel in question due to the absence of the raw data.

3. Results

3.1 Correlation and Covariation between the Reference Shields Stress and Slope

The slope of a mountain river reach is, all things considered, one of the more reliable parameters that can be measured. It is one of the few parameters that can be directly measured from aerial lidar and satellite derived topographic digital elevation models, whereas τ_{*r} is not an easy parameter to measure. The correlation between τ_{*r} and S (Figure 1a) previously observed within a compilation of mountain rivers (Mueller et al., 2005; Lamb et al., 2008) represented a pragmatic path towards estimating a key parameter, even though it lacks the physical basis laid out in the mechanistic models (see Prancevic and Lamb (2015b) for a field application of a mechanistic model). The correlation between S and τ_{*r} has been reported as following both linear and non-linear relations (see Lamb et al., 2008; Mueller et al., 2005; Pitlick et al., 2008; Recking, 2009). We find that the best fit, in a least-squares sense, is a non-linear relation of the form

$$(3)\quad \tau_{*r} = kS^{\alpha},$$

where k=0.27 and α=0.38 (standard error of 0.045) represent the best fit coefficient and exponent (R^2=0.53) for these data, respectively (Figure 1a). This fitted equation is similar to that determined by Pitlick et al. (2008) and possesses a slightly steeper slope than that of Lamb et al. (2008). The differences among the empirical regressions are minor, and arise due to (i) the addition of new field sites present here and (ii) the exclusion of laboratory data from the fit in equation (3). Throughout the rest of the manuscript we will utilize equation (3) when providing examples of τ_{*r} as estimated via an empirical regression, though the issues raised in the following sections are inherent to all such regressions on these or subsets of these data. The non-linear relation provides a better fit to the data, however a linear fit is also reasonable. We also observe that τ_{*bf} possesses a similar non-linear correlation with slope (also observed by Mueller et al., 2005 and Pitlick et al., 2008). The best-fit regression line between τ_{*bf} and S is vertically offset of that between τ_{*r} and S, indicating that τ_{*bf} is slightly larger than τ_{*r} in a consistent manner ($\tau_{*bf}=0.29S^{0.35}$, R^2=0.48 with a standard error of 0.046 for α, Figure 1a). The compilation data represent a larger range of τ_{*bf} and a steeper trend with S ($\tau_{*bf}=0.55S^{0.45}$, R^2=0.28 with a standard error of 0.025 for α).

To understand how the ratio of τ_{*bf}/τ_{*r} computed with measured values compares with the same ratio where τ_{*r} is calculated from the empirical regression we combine equations (1) and (3):

$$\tau_{*bf}/\tau_{*r} \sim \tau_{*bf}/kS^{\alpha} = \frac{hS}{kS^{\alpha}RD_{50}} = \frac{hS^{1-\alpha}}{kRD_{50}}. \quad (4)$$

The primary effect of estimating τ_{*bf}/τ_{*r} with equation (4) is to increase the contribution of slope and minimize the role of the median particle size (for k<1) within the Shields stress. Recall that since the slope is always less than one, as the quantity ($1-\alpha$) approaches zero the slope term approaches a value of one. Using equation (4) the computed average transport capacity is $<\tau_{*bf}/kS^{\alpha}>$=1.26 (arithmetic mean of 1.4), which is close to the observed value of $<\tau_{*bf}/\tau_{*r}>$=1.27 (< > denotes a geometric mean of the bracketed quantity). However, the shape and variance of the distributions are poor matches (Figure 1b), even though equation (4) was fit to these data. Note that equation (4) produces transport capacities that extend well below one, which is a non-physical result as transport was observed in these rivers for sub bankfull flow. The same exercise can be performed for the compilation data using equation (4), which produces an even larger variance (gray PDF in Figure 1b). The larger variance is a result of not capturing the covariation present in τ_{*r} and τ_{*bf}, as each set of observations are pairs. Where τ_{*r} for a given site is larger/smaller relative to equation (3), τ_{*bf} is also larger/smaller for the same site. The covariation between τ_{*bf} and measured τ_{*r} is so strong that no trend is apparent when we take the ratio of τ_{*bf}/τ_{*r} and compare it to S, H/D_{50}, and even τ_{*bf} (Figure 1c). As the required variables to compute τ_{*bf} are commonly available or easier to measure, equations (3) and (4) – or variants thereof – are used frequently to estimate τ_{*r}, despite the fact that the covariation between τ_{*bf} and τ_{*r} produces a spurious result for the transport capacity. Through the use of equation (4) the estimated bankfull transport capacity for both datasets become positively correlated with relative submergence and τ_{*bf}, even though the actual value of τ_{*bf}/τ_{*r} is constant (Figure 1c). These correlations are spurious due to the variables' underlying correlation with slope (Figure 1c). The same degree of correlation is not observed between slope and equation (4), because the relation between H/D_{50} almost precisely cancels out the effect of plotting slope against itself (Figure 1c).

3.2 Parameter Space of the Threshold Field Sites

The second significant issue when computing τ_{*r} with equation (3) results from the partial range of parameter space covered by the field sites from which the regression is based. The broader compilation of field sites represents a more diverse set of gravel rivers and provides context for the range and frequency of the different hydraulic variables (H, S, D_{50}, W, and Q). In general, their probability density histograms do not appear to follow a normal distribution and are better represented by their natural logarithm (Harman et al., 2008). Thus, we natural-log transform the hydraulic variables for the threshold and compilation sites prior to computing the histograms. Compared to the compilation dataset, the threshold site channels are generally shallower, narrower and steeper, with lower bankfull discharges and coarser beds (Figure 2a-f). In other words, sites used for the threshold regressions are a non-representative subset of the larger compilation of gravel rivers. In terms of τ_{*bf}, however, these sites match the central tendency of the larger compilation well (Figure 2f); but they under sample both high and low values of τ_{*bf} relative to the larger compilation. The τ_{*bf} of the compilation appears to be well described by a log-normal distribution yielding a geometric average of $\langle\tau_{*bf}\rangle=0.054$ for single thread coarse-grained rivers (Figure 2f). A two-tailed Kolmogorov-Smirnov test for a log-normal distribution ($K\text{-}S_{stat}=0.045$ with a $P_{value}=0.097$) suggests that we cannot reject the null hypothesis that τ_{*bf} is log-normally distributed (i.e. we accept that τ_{*bf} does not differ from a log-normal distribution at a P_{value} of ~0.1). Additionally, the threshold distribution of τ_{*bf} also follows a log-normal distribution ($K\text{-}S_{stat}=0.095$ with a $P_{value}=0.55$), though not the same distribution as the compilation (Two sample KS-test, $K\text{-}S_{stat}=0.17$ with $P_{value}=0.042$). It is perhaps not surprising that the threshold sites are non-representative of the larger compilation, as these sites are by-and-large geographically biased to mountain rivers primarily within the Rocky Mountains and the states of Colorado, Wyoming, and Idaho whereas the compilation samples a broader geographic range (continental United States and Canada).

The consequences of the geographic bias in measured τ_{*r} and equation (3) can be further explored by removing the self-correlation (slope occurs in both axis) present within Figure (1).

We can examine the relationships between both datasets by exploring the parameter space between H/D_{50} and S, the two free dimensionless variables within Shields stress while holding the quantity $\rho/(\rho_s-\rho)$ constant (Figure 3). When viewed this way the compilation data form a scattered cloud in which bankfull relative submergence (H/D_{50}) trends inversely with slope. These data show that for the same value of τ_{*bf} there exist low gradient rivers with high relative submergence, and steep gradient rivers with low relative submergence. Particularly, these data show that there is quite a range in τ_{*bf}, and that high Shields stresses are not solely the domain of steep rivers. Within this parameter space the threshold sites tend to be overly representative of the steepest rivers (Figure 3). There are few if any threshold field sites occupying the region of the parameter space characterized by low slope, high relative submergence rivers. Within these data a pattern with τ_{*r} emerges showing an additional dependence on H/D (also highlighted by: Mueller et al., 2005; Recking 2009). Equation (3) runs askew to the primary trend of the compilation data, and doesn't capture the overall pattern of τ_{*r} within this parameter space. Interestingly, the pattern in τ_{*r} follows isolines of increasing Shields stress, in that steep rivers with low relative submergence appear to have the same value of τ_{*r} as low gradient rivers with high relative submergence (Figure 3). For example, using equation (3) to estimate τ_{*r} at any value of S would indicate that as H/D_{50} increases so too does the transport capacity of the river. However, the measured values of τ_{*bf}/τ_{*r} do not vary systematically with H/D_{50} or S. From these data it becomes apparent that a third variable, which combines both H/D and S, may be a better predictor of the observed τ_{*r} pattern. However, it is not necessary to fit such a regression as the third variable is the bankfull Shields stress (equation 1).

3.3 Relation between the Bankfull and Reference Shields Stresses

The observed correlation between τ_{*bf} and τ_{*r} is a strong linear trend (Figure 4). It is important to note that the methodology that calculates τ_{*r} is independent of that used to determine τ_{*bf}, as τ_{*r} is determined from a range of flow and flux measurements while τ_{*bf} is determined from channel geometry. The correlation between τ_{*bf} and τ_{*r}, and by extension τ_{*c}, was previously shown (Mueller et al., 2005) to be linear with a subset of the threshold data used here. Mueller et al. (2005) concluded that this trend indicated that gravel-bedded streams were adjusted to have a constant bankfull excess Shields stress (τ_{*bf} - τ_{*c}). The analytic model for the equilibrium channel geometry of gravel-bedded rivers developed by Parker (1978) provides an explanation for the observed correlation and an expected functional form of $\tau_{*bf}=(1+e)\tau_{*c}$, where '*e*' is a small positive value. The prediction for a channel with cohesionless unimodal sediment provides that e=0.2 yielding a predicted relation of $\tau_{*bf}=1.2\tau_{*c}$ for a specified value of τ_{*c}. The best fit relation of this form from the data is $\tau_{*bf}=1.19\tau_{*r}$ (R^2=0.96), which is remarkably close to the analytical prediction (Figure 4). Combining these ideas together provides an avenue to predict τ_{*r} from τ_{*bf} by rearranging the confirmed analytical equation to yield $\tau_{*r}=0.83\tau_{*bf}$. From this relation we can estimate the residuals and compare estimates with equation (3). Histograms of the residuals show a positively skewed distribution from equation (3) and a mostly symmetric and narrower distribution for the analytical prediction (Figure 4 inset).

3.4 Illustration of Perceived Differences in Transport Capacity via Subsampling

To illustrate problems with subsampling the parameter space of gravel bed rivers while using equation (4) to compute the transport capacity, we created a set of contrived subsamples from the larger compilation dataset based on S, H/D_{50}, τ_{*bf}, Q/W, and f (flow resistance). These subsamples are similar to how a researcher might collect field data or values from the literature to compute τ_{*bf}, and through equation (4) estimate the bankfull transport capacity to compare different regions or catchments. It is important to note that selecting field sites within a particular geographic region is something that is commonly done and acceptable practice, but yields a selection of rivers with a limited range in values of S, H/D_{50}, τ_{*bf}, Q/W, and f. Throughout the following exercise we show how application of the slope-based regressions (equation 3) to such data can yield erroneous conclusions. The expected distribution based on the measured τ_{*r} is narrowly distributed around the theoretical prediction (Figure 1b & reproduced in Figure 5a). To facilitate a more direct comparison with the threshold field sites (n=68), we selected 70 random field sites from the full parameter space of the larger compilation (Figure 5a). We chose 70 random samples for the contrived sampling scheme as this number is close to the number of threshold sites, represents a low relative standard error (< 5%), and produces a reasonable distribution. The error in computing the mean is relatively low even for a small set of random samples (Figure 5a), because the natural log-transformed distribution of τ_{*bf} is a normal distribution. The contrived sampling schemes were created by randomly selecting two sets of 70 sites from the compilation dataset from above and below the geometric mean for S, H/D_{50}, τ_{*bf}, and Q/W (Figure 5b), while sampling criteria for f was based on the arithmetic mean value. Flow resistance was computed using the Variable Power Equation $(8/f)^{1/2} = a_1 a_2 (H/D)/[a_1^2 + a_2^2 (H/D)^{5/3}]^{1/2}$ with coefficients a_1=7.3 and a_2=2.3 (Ferguson, 2007), as this equation was previously demonstrated by Ferguson (2007) to match a large compilation of field data well. The final category is a combination of *H/D* and *S* that samples from opposite corners of the compilation parameter space in Figure 3. The differences in transport capacity through the use of equation (4) between the two sets of subsamples for each criterion are illustrated in Figure 5b (see Figure 5c to see the selected sites within the relative submergence-slope parameter space). Some of the contrived subsamples have similar median values for transport capacity to the measured threshold sites; however, all subsamples have substantially larger inner quartile ranges and standard deviations (Figure 5b). Whether a subsample differs from its partner sample is completely dependent on how the selected sites relate to where equation (3) crosses the parameter space (Figure 5c). Subsamples showing little difference from each other are those based on *S* and *Q/W*, while the rest of the subsamples (H/D_{50}, τ_{*bf}, f, H/D_{50} & S) would indicate that transport capacity differs for these sets of gravel rivers. These differences, while statistically significant, are artefacts of the bias that arises by sampling a limited range of the parameter space relative to equation (3).

4. Discussion

Here we start by discussing the quality and bias issues of the threshold data set, as several types of errors are potentially present. The majority of these issues are likely a consequence of the complicated nature of measuring sediment transport and channel hydraulic parameters, which represent snapshots of a dynamic system. For τ_{*bf} the potential sources of error are in determining H, D_{50}, and S at each field site. The largest source of error for this study is related to defining the bankfull depth (Williams, 1978), because errors in both S and D_{50} are less likely to affect the transport capacity as both of these parameters are part of the calculations necessary to compute τ_* and τ_{*r} through equation (2). The error in measuring the bankfull depth is relatively low and decreases with the number of cross sections (Harman et al., 2008), though it remains an open question as to the minimum number of cross sections required to achieve a representative average bankfull depth, and exactly how to treat the bankfull depth (hydraulic radius or average active channel depth) for irregular or complicated cross sections. Our intent is to understand the ratio τ_{*bf}/τ_{*r} as it relates to channel stability, therefore we have chosen to calculate H using the average active channel depth for irregular cross sections and the hydraulic radius where the two metrics closely agree. A full accounting of this problem is not possible given the current datasets, as most field sites have no more than three cross sections from which to compute H; however, the difference between both methods is small, at least for the field sites we have examined here. Defining H as a morphologic break in the channel cross section, we were able to independently reproduce the bankfull depths reported by the original authors of the studies from which the threshold data are compiled. Sources of error for τ_{*r} are potentially more numerous as bed-load transport measurements are notoriously noisy data; for a thorough analysis and discussion of the potential sources of error see Recking (2013). The largest areas of error for the threshold dataset are related to sampling bed-load transport at low transport rates and the choice of sampler used to collect the samples. Mobile samplers (e.g. Helley-Smith) measure higher flux rates for low transport conditions, compared to pit and trap type samplers (Bunte et al., 2008). This oversampling can result in flat (trendless) relations between flux and stress at low transport rates and may have resulted in the exclusion of several field sites where higher transport rates were not available to distinguish a trend. A larger concern with these data is in how representative a single measurement of τ_{*r} is of the threshold, as both the spatial and temporal variability of τ_{*r} remains uncertain. The temporal variability, however, may be less worrisome long term as it appears to be normally distributed where it has been measured (Masteller et al., 2019). Suffice to say, understanding the dynamics of the threshold of motion remains an area in need of additional research. Therefore, we caution the reader from focusing on a single field site or exact numerical values, and instead recommend that the overall trends are more robust.

In terms of data bias of the compilation parameter space coverage, we can only speculate given the available data as to how representative some of these parameters are when compared to the timescales of channel adjustment. In a sense, the reach-scale channel geometry integrates over some yet unknown number of flood events, or may even alternate between different states of adjustment (Pizzuto, 1994; Slater & Singer, 2013; Wolman & Gerson, 1978; Yu & Wolman, 1987). It is not currently definitively known how much the bed composition changes over time and thus how representative a single grain size measurement is, or how sensitive natural channel geometry is to changes in bed composition (e.g. MacKenzie & Eaton, 2017). Similarly, it remains an open question if the sampled bed grain size distribution is reflective of the current measured channel geometry. These are questions though that cannot necessarily be addressed with the current data compilations, but are worth keeping in mind when considering rivers as dynamic systems. In addition, it cannot be definitively concluded that the compilation dataset fully represents the spectrum of τ_{*bf} in coarse-grained rivers, as the compiled field sites necessarily represent the site selection criteria within the original studies. For example, the sampling of field sites is strongly biased geographically towards North America. In particular, field measurements in dryland, arctic or periglacial, and tropical environments are notably lacking. However, given the close fit to a log-normal distribution (Figure 2f) it is not clear to the authors that more globally representative sampling would not simply make any fit better.

Regardless of how representative the compilation dataset is of global rivers, a significant pitfall of using equation (3) to predict τ_{*r} is that the field sites on which equation (3) is based do not sample the full parameter space of the compilation of coarse-grained rivers used in this study (Figure 2 and 3). We note that this is the largest compilation of coarse-grained rivers to date. This uneven sampling is strongly biased towards moderate to high slopes and low relative submergence rivers. Noticeably under sampled are rivers with higher relative submergence for all slopes ($H/D > 20$), and rivers with lower slopes ($S < 0.002$) in general. Caution should be exercised when attempting to extrapolate predictions for τ_{*r} to regions of the parameter space that are not sampled, especially for sites with higher values of H/D relative to equation (3) (Figure 3). Capturing the covariation between τ_{*r} and τ_{*bf} is especially important for estimating bed load transport due to flux equations' non-linear dependence on transport stage (τ_*/τ_{*r}) and/or excess shields stress ($\tau_* - \tau_{*r}$) (Mueller et al., 2005). For example, the difference between $\tau_{*bf}/\tau_{*r} = 1.2$ and $\tau_{*bf}/\tau_{*r} = 2$, seems small given the variation in the data; yet when viewed through a common bed-load transport equation (see Wilcock & Crowe, 2003) this becomes a factor of ~20 in terms of flux and grows non-linearly with increasing values of τ_*/τ_{*r}. As there are very few estimates of τ_{*r} in high Shields stress ($\tau_* > 0.12$) regions of the parameter space, and especially low slope and high relative submergence sites, further research is still required to determine the range of τ_*/τ_{*r} within these regions. The available data do not, however, support the use of equations (3) and (4) to determine τ_{*r} in these regions. These equations would predict that bankfull transport capacity, and hence bed-load flux, increases with τ_{*bf} – despite the available measured data indicating that τ_{*bf}/τ_{*r} ~constant (Figure 1 inset and Figure 4). Interestingly, while the correlation between slope and high values of τ_{*c} is becoming increasingly well understood (see Lamb et al., 2008; Recking, 2009; Prancevic and Lamb, 2015a), to date the explanation for the increase of τ_{*r} with *H/D* for regions of low slope remains uncertain to the authors.

The second issue with the approach laid out in equation (4) is that it does not capture the co-variation between τ_{*b} and τ_{*r} at each site. These two parameters are 'paired' in a sense, and using either fitted regression relation (see figure 1) to estimate τ_{*bf} or τ_{*r} from slope alone will result in an incorrect prediction for the ratio τ_{*bf}/τ_{*r}. This pairing of the data is evident when considering the relation between τ_{*bf} and τ_{*r} (Figure 4), which closely matches theory (Parker, 1978) indicating support for a causative relation. While there is some deviation from this trend within the data (Figure 4) the residuals possess no meaningful correlation with the available hydraulic variables (*H*, *W*, *Q*, *D50*, *H/D*, *f*, and *S*). It remains unclear to the authors if the degree of scatter in τ_{*bf}/τ_{*r} reflects actual ranges of channel behavior, or represents a combination of error or bias in the measurements and under-sampling of the various hydraulic parameters or random noise in a dynamic system. Of the explored relations and correlations, the simple linear relation $\tau_{*bf}=1.2\tau_{*r}$ remains the best predictor to date. In a sense, this model can serve as a null hypothesis. Absent independent measurements of τ_{*c}, this null model states that $\tau_{*bf}=1.2\tau_{*c}$ or $\tau_{*c}=0.83\tau_{*bf}$. With this in mind and the observation that τ_{*bf} is approximately log-normally distributed ($\langle\tau_{*bf}\rangle=0.054$), then τ_{*c} would also be log-normally distributed and we can estimate its mean as $\langle\tau_{*c}\rangle=0.045$ (close to the prediction of the Shields curve). The value in this approximation is that it places statistical bounds on the extent of both τ_{*bf} and τ_{*c} in natural channels. We have demonstrated several potential outcomes of this sampling bias through a variety of field site selection criteria (Figure 5b). Though the demonstrated selection criteria were strictly related to simple statistical splits of hydraulic variables, the discussed bias applies equally to samples drawn based on geography or regional climate. The upshot here is that an empirical slope-based predictor is not broadly reliable for estimating the threshold of motion or predicting the transport capacity, because the data it is based on represent a biased sampling of alluvial gravel rivers and does not account for the covariation between τ_{*bf} and τ_{*r}. We advocate that τ_{*r} can be estimated from τ_{*bf} due to the remarkable consistency observed in channel geometry and the close connection to theory which provides a physical basis for the prediction. Using channel geometry to predict the threshold of motion provides an implicitly time and space averaged reach-scale value for τ_{*c}, however the extent of the averaging will depend on the number of flows responsible for shaping the current channel geometry.

Lacking an alternative easily implementable approach to predicting τ_{*c}, we recommend using the null model (τ_{*bf}/τ_{*c}=1.2) in theory, numerical, and analytical based approaches, while for strictly empirical approaches error can be incorporated through the observed distribution and standard deviation ($<\tau_{*bf}/\tau_{*r}>=1.27 \times/\div 1.16$). The null model provides a closure for studies in gravel-bed rivers where τ_{*c} needs to be estimated. For example, predicting spatial patterns of grain size and morphology for in stream management and habitat suitability (Phillips & Scatena, 2013; Snyder et al., 2013), and management of river corridors below major river modifications (Minear, 2010; Schmidt & Wilcock, 2008). For field sites where the identification of the bankfull depth is difficult to assess we recommend checking the data against the compilation dataset parameter space (Figure 3) for a variety of flow depths to assess a likely range. This approach is also insightful to assess potential bias for geographically based sampling. For steeper river channels ($S > 0.01$ and $H/D < 10$) where one absolutely requires an approximation of τ_{*r} based on metrics extracted from topography alone, the slope-based regression in equation (3) and other published variants may be suitable with the former caveats in mind. We recommend the field based empirical regressions over those that incorporate laboratory measurements, because the field based regressions capture processes (and errors) inherent to the field that are absent in the lab such as the difference between measured particle size and mass in steep channels (see Miller et al., 2014). We do not have a recommendation for bedrock rivers, as the concept of bankfull does not always exist and a bankfull analogue with morphological significance has yet to be fully established. Research in this area is still developing, however field and flume experiments (Johnson et al., 2009; Johnson & Whipple, 2010) have demonstrated that bedrock rivers appear to adjust towards a condition of steady state to pass the sediment flux and water discharge supplied. This is similar to the statistical concept of the ‘effective flood’ in alluvial rivers which is a bankfull analogue and represents the average stress above the threshold of motion (Phillips & Jerolmack, 2016; Torizzo & Pitlick, 2004; Wolman & Miller, 1960).

5. Conclusion

Through the use of an expanded dataset, we demonstrate that empirical regressions based on the correlation between slope and the threshold of motion can easily result in erroneous conclusions when considering the channel's transport capacity. This occurs because the empirical regressions are based on a limited sampling of the parameter space of bed-load rivers and do not capture the covariation between τ_{*bf} and τ_{*r}. Predicting the threshold of motion in natural channels remains a considerable challenge, and a critical knowledge gap for understanding rivers' roles within their catchments. We recommend site-specific empirical determination of the threshold from independent measurements of bed-load transport; while this is challenging, the rapid uptake of seismic, acoustic, and other methods makes this prospect increasingly more feasible. Barring direct measurement, the threshold of motion's strong correlation with the bankfull Shields stress remains the most accurate predictor. The covariation of threshold and bankfull Shields stresses is a consequence of the organization of bed-load rivers to be close to the threshold of motion. The average bankfull transport capacity determined from available data is in remarkable agreement with the prevailing theory for gravel-bed river geometry (Parker, 1978). Observed deviation from this theory when using these empirical regressions is an artefact of the sampling bias inherent in their construction; future studies will need to address this bias rigorously with independent observations of the threshold in order to disprove the null hypothesis.

Acknowledgements

Research was supported by the NSF INSPIRE program (EAR-1344280), a NSF-Postdoctoral Fellowship (EAR-1349776) and a Nature Conservancy NatureNet Fellowship (P105251) awarded to CBP, and through an Army Research Office grant (W911-NF-16-1-0290) to DJJ. We thank the Associate Editor, J. Prancevic, J. Johnson, and an anonymous reviewer for thorough and constructive reviews that improved this manuscript. New data compiled within this study are available as supplemental material, while the larger compilation of river geometry is publicly available from the original sources.

References

Andrews, E. D. (1994). Marginal bed load transport in a gravel bed stream, Sagehen Creek, California. *Water Resources Research*, *30*(7), 2241–2250. https://doi.org/10.1029/94WR00553

Andrews, E. D. (2000). Bed material transport in the Virgin River, Utah. *Water Resources Research*, *36*(2), 585–596. https://doi.org/10.1029/1999WR900257

Andrews, E. D., & Erman, D. C. (1986). Persistence in the Size Distribution of Surficial Bed Material During an Extreme Snowmelt Flood. *Water Resources Research*, *22*(2), 191–197. https://doi.org/10.1029/WR022i002p00191

Barton, J. (2006). *Passive acoustic monitoring of coarse bedload in mountain streams* (Ph.D.). The Pennsylvania State University, State College, PA.

Buffington, J. M., & Montgomery, D. R. (1997). A systematic analysis of eight decades of incipient motion studies, with special reference to gravel-bedded rivers. *Water Resources Research*, *33*(8), PP. 1993–2029. https://doi.org/199710.1029/96WR03190

Bunte, K. (1998). *Development and field testing of a stationary net-frame bedload sampler for measuring entrainment of pebble and cobble particles* (Report) (p. 74). Fort Collins, CO: Stream System Technology Center, Rocky Mountain Research Station, U.S. Dept. of Agriculture Forest Service.

Bunte, K., Abt, S. R., Potyondy, J. P., & Swingle, K. W. (2008). A Comparison of Coarse Bedload Transport Measured with Bedload Traps and Helley-Smith Samplers. *Geodinamica Acta*, *21*(1–2), 53–66. https://doi.org/10.3166/ga.21.53-66

Bunte, K., Abt, S. R., Swingle, K. W., Cenderelli, D. A., & Schneider, J. M. (2013). Critical shields values in coarse-bedded steep streams. *Water Resources Research*, 7427–7447. https://doi.org/10.1002/2012WR012672

Charru, F., Mouilleron, H., & Eiff, O. (2004). Erosion and deposition of particles on a bed sheared by a viscous flow. *Journal of Fluid Mechanics*, *519*, 55–80. https://doi.org/10.1017/S0022112004001028

Church, M., & Rood, K. (1983). *Catalogue of alluvial river channel regime data*. Vancouver: University of British Columbia.

Dade, W. B., & Friend, P. F. (1998). Grain-size, sediment-transport regime, and channel slope in alluvial rivers. *Journal of Geology*, *106*(6), 661.

Dunne, K. B. J., & Jerolmack, D. J. (2018). Evidence of, and a proposed explanation for, bimodal transport states in alluvial rivers. *Earth Surface Dynamics*, *6*(3), 583–594. https://doi.org/10.5194/esurf-6-583-2018

Erwin, S. O., Schmidt, J. C., & Nelson, N. C. (2011). Downstream effects of impounding a natural lake: the Snake River downstream from Jackson Lake Dam, Wyoming, USA. *Earth Surface Processes and Landforms*, *36*(11), 1421–1434. https://doi.org/10.1002/esp.2159

Ferguson, R. I. (2007). Flow resistance equations for gravel- and boulder-bed streams. *Water Resources Research*, *43*, 12 PP. https://doi.org/200710.1029/2006WR005422

Ferguson, R. I. (2012). River channel slope, flow resistance, and gravel entrainment thresholds. *Water Resources Research*, *48*(5), W05517. https://doi.org/10.1029/2011WR010850

Ferguson, R. I., & Church, M. (2009). A critical perspective on 1-D modeling of river processes: Gravel load and aggradation in lower Fraser River. *Water Resources Research*, *45*(11). https://doi.org/10.1029/2009WR007740

Freedman, D., & Diaconis, P. (1981). On the histogram as a density estimator: L2 theory. *Zeitschrift Für Wahrscheinlichkeitstheorie Und Verwandte Gebiete*, *57*(4), 453–476. https://doi.org/10.1007/BF01025868

Glover, R. E., & Florey, Q. L. (1951). *Stable channel profiles* (Tech. Rep. U.S. Bur. Reclamation). Denver, CO. USA.

Gray, J. R., Laronne, J. B., & Marr, J. D. G. (2010). *Bedload-surrogate monitoring technologies* (U.S. Geological Survey Scientific Investigations Report No. 2010–5091) (p. 37). United States Geological Survey.

Harman, C., Stewardson, M., & DeRose, R. (2008). Variability and uncertainty in reach bankfull hydraulic geometry. *Journal of Hydrology*, *351*(1), 13–25. https://doi.org/10.1016/j.jhydrol.2007.11.015

Hempel, L. A. (2018). *The Effects of the Flow Regime on Stream Channel Form and Processes* (Ph.D.). Oregon State University, Corvalis, OR.

Henderson, F. M. (1963). Stability of alluvial channels. *T. Am. Soc. Civ. Eng.*, *128*, 657–686.

Hinton, D., Hotchkiss, R., & Ames, D. P. (2017). Comprehensive and Quality-Controlled Bedload Transport Database. *Journal of Hydraulic Engineering*, *143*(2), 06016024. https://doi.org/10.1061/(ASCE)HY.1943-7900.0001221

Houssais, M., Ortiz, C. P., Durian, D. J., & Jerolmack, D. J. (2015). Onset of sediment transport is a continuous transition driven by fluid shear and granular creep. *Nature Communications*, *6*, 6527. https://doi.org/10.1038/ncomms7527

Hsu, L., Finnegan, N. J., & Brodsky, E. E. (2011). A seismic signature of river bedload transport during storm events. *Geophysical Research Letters*, *38*. https://doi.org/10.1029/2011GL047759

Johnson, J. P. L. (2016). Gravel threshold of motion: a state function of sediment transport disequilibrium? *Earth Surface Dynamics*, *4*(3), 685–703. https://doi.org/10.5194/esurf-4-685-2016

Johnson, J. P. L., & Whipple, K. X. (2010). Evaluating the controls of shear stress, sediment supply, alluvial cover, and channel morphology on experimental bedrock incision rate. *Journal of Geophysical Research-Earth Surface*, *115*. https://doi.org/10.1029/2009JF001335

Johnson, J. P. L., Whipple, K. X., Sklar, L. S., & Hanks, T. C. (2009). Transport slopes, sediment cover, and bedrock channel incision in the Henry Mountains, Utah. *Journal of Geophysical Research*, *114*, 21 PP. https://doi.org/200910.1029/2007JF000862

Jones, M. L., & Seitz, H. R. (1980). *Sediment transport in the Snake and Clearwater rivers in the vicinity of Lewiston, Idaho* (No. OFR-80-690). United States Geological Survey.

King, J. G., Emmett, W. W., Whiting, P. J., Kenworthy, R. P., & Barry, J. J. (2004). *Sediment transport data and related information for selected coarse-bed streams and rivers in Idaho* (No. Gen. Tech. Rep. RMRS-GTR-131). Fort Collins, CO: U.S. Department of Agriculture, Forest Service, Rocky Mountain Research Station.

Kirchner, J. W., Dietrich, W. E., Iseya, F., & Ikeda, H. (1990). The variability of critical shear stress, friction angle, and grain protrusion in water worked sediments. *Sedimentology*, *37*, 647–672.

Lamb, M. P., Dietrich, W. E., & Venditti, J. G. (2008). Is the critical Shields stress for incipient sediment motion dependent on channel-bed slope? *Journal of Geophysical Research: Earth Surface*, *113*(F2), F02008. https://doi.org/10.1029/2007JF000831

Lamb, M. P., Brun, F., & Fuller, B. M. (2017a). Direct measurements of lift and drag on shallowly submerged cobbles in steep streams: Implications for flow resistance and sediment transport. *Water Resources Research*, *53*(9), 7607–7629. https://doi.org/10.1002/2017WR020883

Lamb, M. P., Brun, F., & Fuller, B. M. (2017b). Hydrodynamics of steep streams with planar coarse-grained beds: Turbulence, flow resistance, and implications for sediment transport. *Water Resources Research*, *53*(3), 2240–2263. https://doi.org/10.1002/2016WR019579

Leopold, L. B., & Maddock, T. (1953). The Hydraulic Geometry of Stream Channels and Some Physiographic Implications. *U.S. Geological Survey Professional Paper*, *252*. https://doi.org/10.3133/pp252

Leopold, L. B., & Wolman, M. G. (1957). *River Channel Patterns: Braided, Meandering, and Straight* (No. PP-282-B). United States Geological Survey.

Li, C., Czapiga, M. J., Eke, E. C., Viparelli, E., & Parker, G. (2014). Variable Shields number model for river bankfull geometry: bankfull shear velocity is viscosity-dependent but grain size-independent. *Journal of Hydraulic Research*, *0*(0), 1–13. https://doi.org/10.1080/00221686.2014.939113

Lisle, T. E., Nelson, J. M., Pitlick, J., Madej, M. A., & Barkett, B. L. (2000). Variability of bed mobility in natural, gravel-bed channels and adjustments to sediment load at local and reach scales. *Water Resources Research*, *36*(12), 3743–3755. https://doi.org/10.1029/2000WR900238

MacKenzie, L. G., & Eaton, B. C. (2017). Large grains matter: contrasting bed stability and morphodynamics during two nearly identical experiments. *Earth Surface Processes and Landforms*, *42*(8), 1287–1295. https://doi.org/10.1002/esp.4122

Marquis, G. A., & Roy, A. G. (2012). Using multiple bed load measurements: Toward the identification of bed dilation and contraction in gravel-bed rivers. *Journal of Geophysical Research*, *117*(F1), F01014. https://doi.org/10.1029/2011JF002120

Masteller, C. C., & Finnegan, N. J. (2017). Interplay between grain protrusion and sediment entrainment in an experimental flume. *Journal of Geophysical Research: Earth Surface*, *122*(1), 2016JF003943. https://doi.org/10.1002/2016JF003943

Masteller, C. C., Finnegan, N. J., Turowski, J. M., Yager, E. M., & Rickenmann, D. (2019). History-Dependent Threshold for Motion Revealed by Continuous Bedload Transport Measurements in a Steep Mountain Stream. *Geophysical Research Letters*, *46*(5), 2583–2591. https://doi.org/10.1029/2018GL081325

May, C. L., & Pryor, B. S. (2013). Initial Motion and Bedload Transport Distance Determined by Particle Tracking in a Large Regulated River. *River Research and Applications*, *30*(4), 508–520. https://doi.org/10.1002/rra.2665

May, C. L., Pryor, B., Lisle, T. E., & Lang, M. (2009). Coupling hydrodynamic modeling and empirical measures of bed mobility to predict the risk of scour and fill of salmon redds in a large regulated river. *Water Resources Research*, *45*(5). https://doi.org/10.1029/2007WR006498

McLean, D. G., Church, M., & Tassone, B. (1999). Sediment transport along lower Fraser River: 1. Measurements and hydraulic computations. *Water Resources Research*, *35*(8), 2533–2548. https://doi.org/10.1029/1999WR900101

Métivier, F., Lajeunesse, E., & Devauchelle, O. (2017). Laboratory rivers: Lacey's law, threshold theory, and channel stability. *Earth Surface Dynamics*, *5*(1), 187–198. https://doi.org/10.5194/esurf-5-187-2017

Milhous, R. T. (1973). *Sediment transport in a gravel-bottomed stream* (Ph.D.). Oregon State University, Corvalis, OR.

Miller, K. L., Szabó, T., Jerolmack, D. J., & Domokos, G. (2014). Quantifying the significance of abrasion and selective transport for downstream fluvial grain size evolution. *Journal of Geophysical Research: Earth Surface*, *119*(11), 2412–2429. https://doi.org/10.1002/2014JF003156

Minear, J. T. (2010). *The Downstream Geomorphic Effects of Dams: A Comprehensive and Comparative Approach*. UC Berkeley. Retrieved from https://escholarship.org/uc/item/1f8612f9

Monsalve, A., Yager, E. M., Turowski, J. M., & Rickenmann, D. (2016). A probabilistic formulation of bed load transport to include spatial variability of flow and surface grain size distributions. *Water Resources Research*, *52*(5), 3579–3598. https://doi.org/10.1002/2015WR017694

Mueller, E. R., & Pitlick, J. (2014). Sediment supply and channel morphology in mountain river systems: 2. Single thread to braided transitions. *Journal of Geophysical Research: Earth Surface*, *119*(7), 2013JF003045. https://doi.org/10.1002/2013JF003045

Mueller, E. R., Pitlick, J., & Nelson, J. M. (2005). Variation in the reference Shields stress for bed load transport in gravel-bed streams and rivers. *Water Resources Research*, *41*(4), W04006. https://doi.org/10.1029/2004WR003692

Paola, C., & Seal, R. (1995). Grain-Size Patchiness as a Cause of Selective Deposition and Downstream Fining. *Water Resources Research*, *31*(5), 1395–1407. https://doi.org/10.1029/94WR02975

Parker, G. (1978). Self-formed straight rivers with equilibrium banks and mobile bed. Part 2 The gravel river. *Journal of Fluid Mechanics*, *89*(1), 127–146.

Parker, G. (1979). Hydraulic Geometry of Active Gravel Rivers. *Journal of the Hydraulics Division-Asce*, *105*(9), 1185–1201.

Parker, G. (1990). Surface-based bedload transport relation for gravel rivers. *Journal of Hydraulic Research*, *28*(4), 417. https://doi.org/10.1080/00221689009499058

Parker, G., Klingeman, P., & Mclean, D. (1982). Bedload and Size Distribution in Paved Gravel-Bed Streams. *Journal of the Hydraulics Division-Asce*, *108*(4), 544–571.

Parker, G., Wilcock, P. R., Paola, C., Dietrich, W. E., & Pitlick, J. (2007). Physical basis for quasi-universal relations describing bankfull hydraulic geometry of single-thread gravel bed rivers. *Journal of Geophysical Research*, *112*, 21 PP. https://doi.org/200710.1029/2006JF000549

Pender, G., Shvidchenko, A. B., & Chegini, A. (2007). Supplementary data confirming the relationship between critical Shields stress, grain size and bed slope. *Earth Surface Processes and Landforms*, *32*(11), 1605–1610. https://doi.org/10.1002/esp.1588

Pfeiffer, A. M., Finnegan, N. J., & Willenbring, J. K. (2017). Sediment supply controls equilibrium channel geometry in gravel rivers. *Proceedings of the National Academy of Sciences*, *114*(13), 3346–3351. https://doi.org/10.1073/pnas.1612907114

Phillips, C. B., & Jerolmack, D. J. (2014). Dynamics and mechanics of bed-load tracer particles. *Earth Surface Dynamics*, *2*(2), 513–530. https://doi.org/10.5194/esurf-2-513-2014

Phillips, C. B., & Jerolmack, D. J. (2016). Self-organization of river channels as a critical filter on climate signals. *Science*, *352*(6286), 694–697. https://doi.org/10.1126/science.aad3348

Phillips, C. B., & Scatena, F. N. (2013). Reduced channel morphological response to urbanization in a flood-dominated humid tropical environment. *Earth Surface Processes and Landforms*, *38*(9), 970–982. https://doi.org/10.1002/esp.3345

Phillips, C. B., Martin, R. L., & Jerolmack, D. J. (2013). Impulse framework for unsteady flows reveals superdiffusive bed load transport. *Geophysical Research Letters*, *40*(7), 1328–1333. https://doi.org/10.1002/grl.50323

Phillips, C. B., Hill, K. M., Paola, C., Singer, M. B., & Jerolmack, D. J. (2018). Effect of Flood Hydrograph Duration, Magnitude, and Shape on Bed Load Transport Dynamics. *Geophysical Research Letters*, *45*, 8264–8271. https://doi.org/10.1029/2018GL078976

Pitlick, J., & Cress, R. (2002). Downstream changes in the channel geometry of a large gravel bed river. *Water Resources Research*, *38*(10), 34–1–34–11. https://doi.org/10.1029/2001WR000898

Pitlick, J., Mueller, E. R., Segura, C., Cress, R., & Torizzo, M. (2008). Relation between flow, surface-layer armoring and sediment transport in gravel-bed rivers. *Earth Surface Processes and Landforms*, *33*(8), 1192–1209. https://doi.org/10.1002/esp.1607

Pitlick, J., Marr, J., & Pizzuto, J. (2013). Width adjustment in experimental gravel-bed channels in response to overbank flows. *Journal of Geophysical Research-Earth Surface*, *118*(2), 553–570. https://doi.org/10.1002/jgrf.20059

Pizzuto, J. E. (1994). Channel adjustments to changing discharges, Powder River, Montana. *GSA Bulletin*, *106*(11), 1494–1501. https://doi.org/10.1130/0016-7606(1994)106<1494:CATCDP>2.3.CO;2

Prancevic, J. P., & Lamb, M. P. (2015a). Particle friction angles in steep mountain channels. *Journal of Geophysical Research: Earth Surface*, *120*(2), 2014JF003286. https://doi.org/10.1002/2014JF003286

Prancevic, J. P., & Lamb, M. P. (2015b). Unraveling bed slope from relative roughness in initial sediment motion. *Journal of Geophysical Research: Earth Surface*, *120*(3), 2014JF003323. https://doi.org/10.1002/2014JF003323

Prancevic, J. P., Lamb, M. P., & Fuller, B. M. (2014). Incipient sediment motion across the river to debris-flow transition. *Geology*, *42*(3), 191–194. https://doi.org/10.1130/G34927.1

Rankl, J. G., & Smalley, M. L. (1992). *Transport of sediment by streams in the Sierra Madre, southern Wyoming* (USGS Numbered Series No. 92–4091). U.S. Geological Survey; Open-File Reports.

Recking, A. (2009). Theoretical development on the effects of changing flow hydraulics on incipient bed load motion. *Water Resources Research*, *45*(4), W04401. https://doi.org/10.1029/2008WR006826

Recking, A. (2010). A comparison between flume and field bed load transport data and consequences for surface-based bed load transport prediction. *Water Resources Research*, *46*. https://doi.org/10.1029/2009WR008007

Recking, A. (2013). An analysis of nonlinearity effects on bed load transport prediction. *Journal of Geophysical Research: Earth Surface*, *118*(3), 1264–1281. https://doi.org/10.1002/jgrf.20090

Reid, I., Frostick, L. E., & Layman, J. T. (1985). The incidence and nature of bedload transport during flood flows in coarse-grained alluvial channels. *Earth Surface Processes and Landforms*, *10*(1), 33–44. https://doi.org/10.1002/esp.3290100107

Reitz, M. D., Jerolmack, D. J., Lajeunesse, E., Limare, A., Devauchelle, O., & Métivier, F. (2014). Diffusive evolution of experimental braided rivers. *Physical Review E*, *89*(5), 052809. https://doi.org/10.1103/PhysRevE.89.052809

Rickenmann, D., Turowski, J. M., Fritschi, B., Klaiber, A., & Ludwig, A. (2012). Bedload transport measurements at the Erlenbach stream with geophones and automated basket samplers. *Earth Surface Processes and Landforms*, *37*(9), 1000–1011. https://doi.org/10.1002/esp.3225

Roth, D. L., Brodsky, E. E., Finnegan, N. J., Rickenmann, D., Turowski, J. M., & Badoux, A. (2016). Bed load sediment transport inferred from seismic signals near a river. *Journal of Geophysical Research: Earth Surface*, *121*(4), 725–747. https://doi.org/10.1002/2015JF003782

Ryan, S. E., & Emmett, W. W. (2002). The nature of flow and sediment movement in Little Granite Creek near Bondurant, Wyoming. *Gen. Tech. Rep. RMRS-GTR-90. Ogden, UT: U.S. Department of Agriculture, Forest Service, Rocky Mountain Research Station. 48 p.*, *090*. https://doi.org/10.2737/RMRS-GTR-90

Ryan, S. E., Porth, L. S., & Troendle, C. A. (2005). Coarse sediment transport in mountain streams in Colorado and Wyoming, USA. *Earth Surface Processes and Landforms*, *30*(3), 269–288. https://doi.org/10.1002/esp.1128

Schmidt, J. C., & Wilcock, P. R. (2008). Metrics for assessing the downstream effects of dams. *Water Resources Research*, *44*(4). https://doi.org/10.1029/2006WR005092

Schumm, S. A. (1960). *The Shape of Alluvial Channels in Relation To Sediment Type* (Geological Survey Professional Paper No. 352- B).

Seizilles, G., Lajeunesse, E., Devauchelle, O., & Bak, M. (2014). Cross-stream diffusion in bedload transport. *Physics of Fluids (1994-Present)*, *26*(1), 013302. https://doi.org/10.1063/1.4861001

Shields, A. (1936). *Application of similarity principles and turbulence research to bed-load movement* (Ph.D.). Mitt. Preuss. Vers. Wasserbau Schiffbau.

Shvidchenko, A. B., & Pender, G. (2000). Flume study of the effect of relative depth on the incipient motion of coarse uniform sediments. *Water Resources Research*, *36*(2), 619–628. https://doi.org/10.1029/1999WR900312

Slater, L. J., & Singer, M. B. (2013). Imprint of climate and climate change in alluvial riverbeds: Continental United States, 1950-2011. *Geology*, *41*(5), 595–598. https://doi.org/10.1130/G34070.1

Slater, L. J., Singer, M. B., & Kirchner, J. W. (2015). Hydrologic versus geomorphic drivers of trends in flood hazard. *Geophysical Research Letters*, *42*(2), 370–376. https://doi.org/10.1002/2014GL062482

Smalley, M. L., Emmett, W. W., & Wacker, A. M. (1994). *Annual replenishment of bed material by sediment transport in the Wind River near Riverton, Wyoming* (USGS Numbered Series No. 94–4007). U.S. Geological Survey; USGS Earth Science Information Center, Open-File Reports Section.

Snyder, N. P., Nesheim, A. O., Wilkins, B. C., & Edmonds, D. A. (2013). Predicting grain size in gravel-bedded rivers using digital elevation models: Application to three Maine watersheds. *GSA Bulletin*, *125*(1–2), 148–163. https://doi.org/10.1130/B30694.1

Torizzo, M., & Pitlick, J. (2004). Magnitude-frequency of bed load transport in mountain streams in Colorado. *Journal of Hydrology*, *290*(1–2), 137–151. https://doi.org/10.1016/j.jhydrol.2003.12.001

Trampush, S. M., Huzurbazar, S., & McElroy, B. (2014). Empirical assessment of theory for bankfull characteristics of alluvial channels. *Water Resources Research*, *50*(12), 9211–9220. https://doi.org/10.1002/2014WR015597

Turowski, J. M., Badoux, A., & Rickenmann, D. (2011). Start and end of bedload transport in gravel-bed streams. *Geophysical Research Letters*, *38*, 5 PP. https://doi.org/201110.1029/2010GL046558

Whitaker, A. C., & Potts, D. F. (2007). Coarse bed load transport in an alluvial gravel bed stream, Dupuyer Creek, Montana. *Earth Surface Processes and Landforms*, *32*(13), 1984–2004. https://doi.org/10.1002/esp.1512

Wiberg, P. L., & Smith, J. D. (1987). Calculations of the Critical Shear Stress for Motion of Uniform and Heterogeneous Sediments. *Water Resources Research*, *23*(8), 1471–1480. https://doi.org/10.1029/WR023i008p01471

Wilcock, P. R. (1992). Flow competence: A criticism of a classic concept. *Earth Surface Processes and Landforms*, *17*(3), 289–298. https://doi.org/10.1002/esp.3290170307

Wilcock, P. R. (1998). Two-Fraction Model of Initial Sediment Motion in Gravel-Bed Rivers. *Science*, *280*(5362), 410–412. https://doi.org/10.1126/science.280.5362.410

Wilcock, P. R., & Crowe, J. C. (2003). Surface-based Transport Model for Mixed-Size Sediment. *Journal of Hydraulic Engineering*, *129*(2), 120.

Wilcock, P. R., & McArdell, B. W. (1997). Partial transport of a sand/gravel sediment. *Water Resources Research*, *33*(1), 235–245. https://doi.org/10.1029/96WR02672

Wilcock, P. R., Barta, A. F., Shea, C. C., Kondolf, G. M., Matthews, W. V. G., & Pitlick, J. (1996). Observations of Flow and Sediment Entrainment on a Large Gravel-Bed River. *Water Resources Research*, *32*(9), P. 2897. https://doi.org/199610.1029/96WR01628

Williams, G. P. (1978). Bank-full discharge of rivers. *Water Resources Research*, *14*(6), 1141–1154. https://doi.org/10.1029/WR014i006p01141

Wolman, M. G., & Gerson, R. (1978). Relative scales of time and effectiveness of climate in watershed geomorphology. *Earth Surface Processes*, *3*(2), 189–208. https://doi.org/10.1002/esp.3290030207

Wolman, M. G., & Miller, J. P. (1960). Magnitude and Frequency of Forces in Geomorphic Processes. *The Journal of Geology*, *68*(1), 54–74.

Yager, E. M., Turowski, J. M., Rickenmann, D., & McArdell, B. W. (2012). Sediment supply, grain protrusion, and bedload transport in mountain streams. *Geophysical Research Letters*, *39*. https://doi.org/10.1029/2012GL051654

Yager, E. M., Schmeeckle, M. W., & Badoux, A. (2018). Resistance Is Not Futile: Grain Resistance Controls on Observed Critical Shields Stress Variations. *Journal of Geophysical Research: Earth Surface*, *123*(12), 3308–3322. https://doi.org/10.1029/2018JF004817

Yu, B., & Wolman, M. G. (1987). Some dynamic aspects of river geometry. *Water Resources Research*, *23*(3), 501–509. https://doi.org/10.1029/WR023i003p00501

Zimmermann, A., Church, M., & Hassan, M. A. (2010). Step-pool stability: Testing the jammed state hypothesis. *Journal of Geophysical Research: Earth Surface*, *115*(F2). https://doi.org/10.1029/2009JF001365

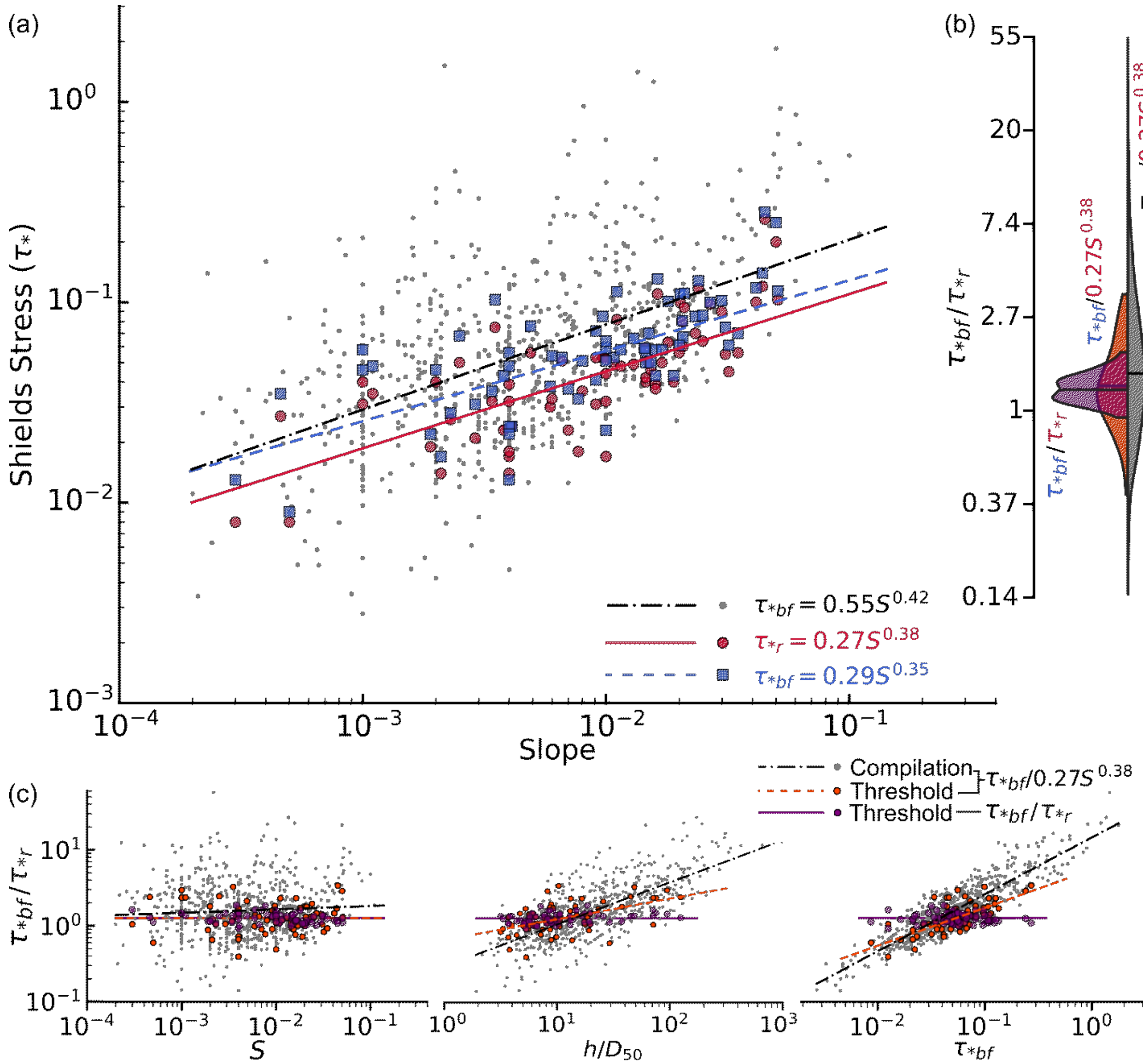

Figure 1. Correlation between slope, bankfull Shields stress, and the threshold of motion. (a) Observed correlation for the threshold data between reach-scale slope, and the reference (τ_{*r}, red circles) and bankfull Shields stresses (τ_{*bf}, blue squares). Red (solid) and blue (dashed) lines represent loglog least-squares regressions excluding two outliers (τ_{*r}>0.2). Gray points represent τ_{*bf} for the compilation data with a least-squares regression line (black dash-dot line). (b) Split violin plot of the distributions of the bankfull transport capacity (τ_{*bf}/τ_{*r}) where τ_{*r} is estimated from flux measurements (purple), and the slope-based regression ($\tau_{*r}=0.27S^{0.38}$) for the threshold (orange) and compilation data (gray). The solid line within the distribution represents the median and the the upper and lower edges of the distribution are clipped at the extents of the data. (c) Relations between slope, bankfull relative submergence (H/D_{50}), and τ_{*bf} with τ_{*bf}/τ_{*r} for the

threshold (purple and orange circles) and compilation data (gray points). Horizontal lines represent the geometric mean ($\langle\tau_{*bf}/\tau_{*r}\rangle=1.27$) where there is no correlation between the data. Note that the trends observed for H/D_{50} and τ_{*bf} result from spurious correlation with slope within equation (4).

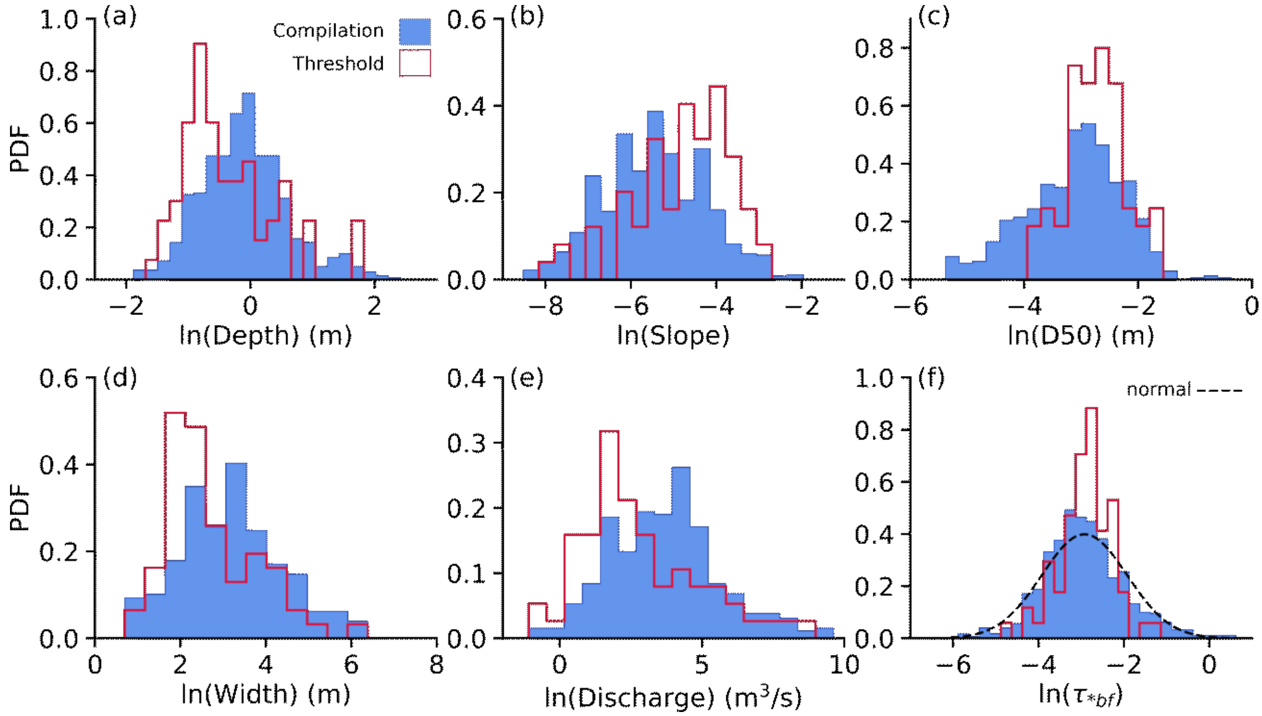

Figure 2. Probability density histograms for sites where τ_{*r} was determined from bed-load flux measurements (red line, n=68) compared with a larger data compilation (shaded blue, n=739) of gravel-bedded rivers. All data were natural-log transformed prior to computing the histograms and bin width for both datasets used the Freedman-Diaconis rule (Freedman & Diaconis, 1981) based on the larger compilation. The variables are (a) bankfull depth (n=725), (b) slope (n=739), (c) D_{50} (n=739), (d) bankfull width (n=272), (e) bankfull discharge (n=418), and (f) bankfull Shields stress (n=725). Sample sizes vary according to data availability. The bankfull Shields stress (f) is well described by a normal distribution (black dashed line) in natural log space.

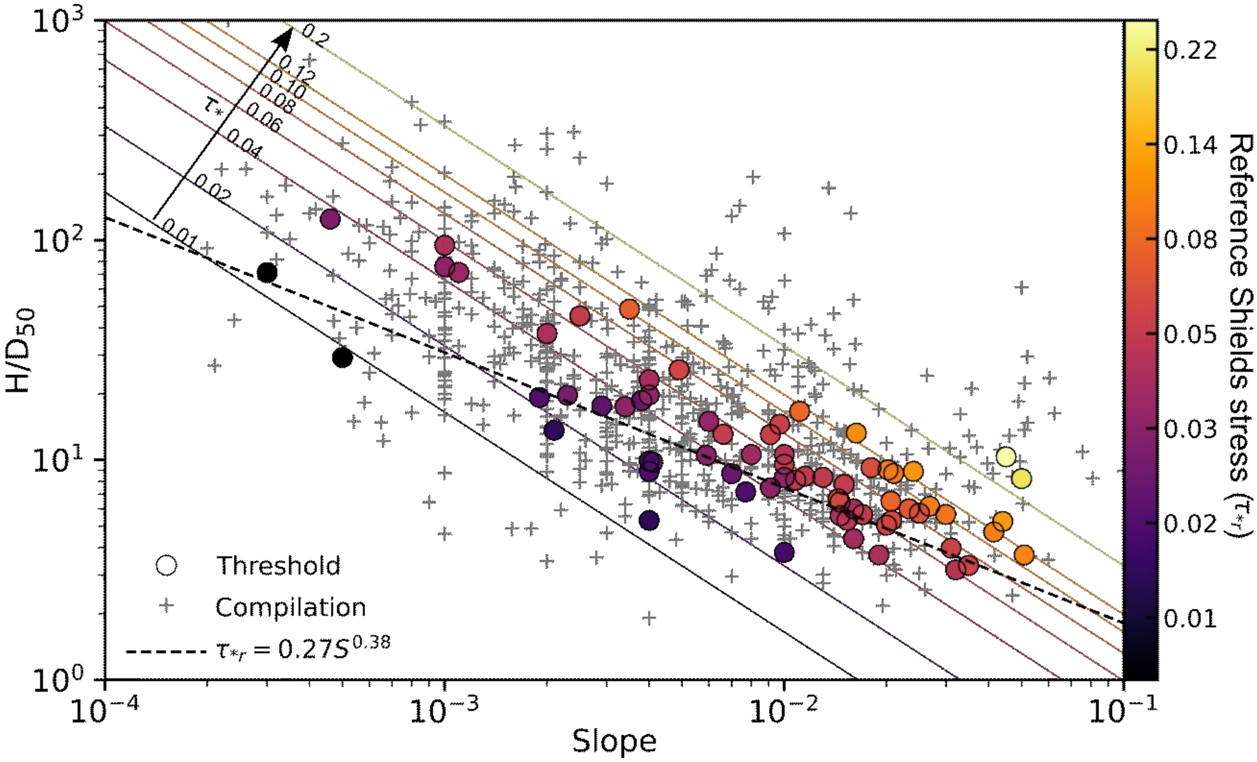

Figure 3. Parameter space of bankfull relative submergence (H/D_{50}) and slope for sites with measured τ_{*r} (shaded circles) and the larger river compilation (gray '+' symbol). The shaded color and colorbar denote the measured reference Shields stress. The black dashed line represents the best fit regression between slope and τ_{*r} (equation 3). The multicolored diagonal lines are, by definition, the Shields stress. Note that the shaded color pattern is parallel to the Shields stress isolines (i.e. light orange points follow the orange isolines and the purple points follow the purple lines) and not the regression line.

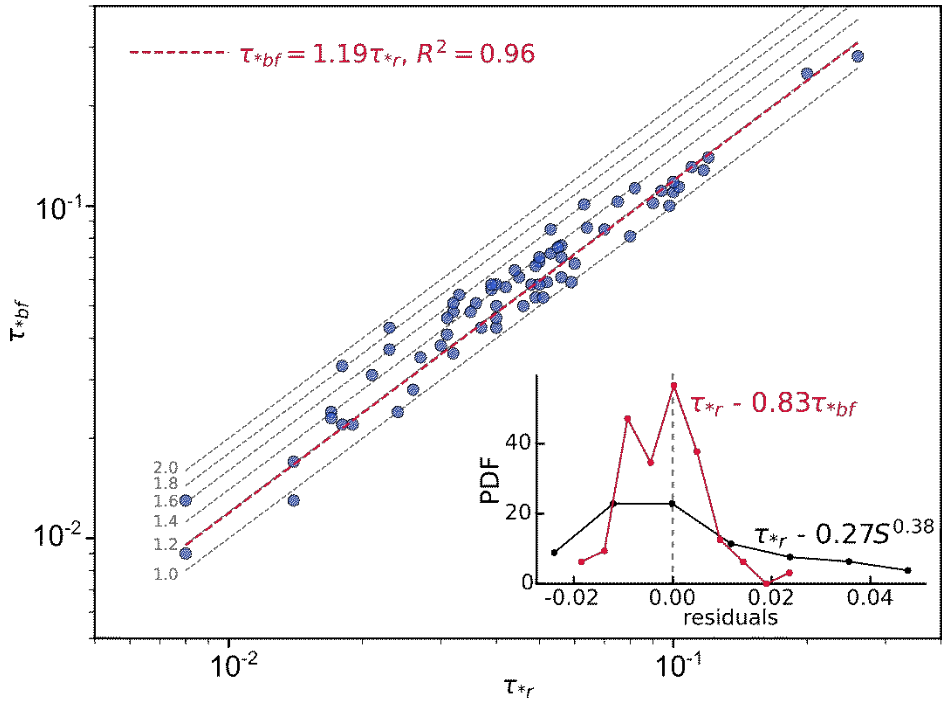

Figure 4. Relation between the reference and the bankfull Shields stresses. The gray dashed lines represent increasing values for the ratio τ_{*bf}/τ_{*r} in increments of 0.2 for reference, while the red dashed line represents the best fit function of the form $\tau_{*bf}=(1+e)\tau_{*r}$. (inset) Residuals for estimating τ_{*r} using the relation with τ_{*bf} (red line) and equation (3) (black line).

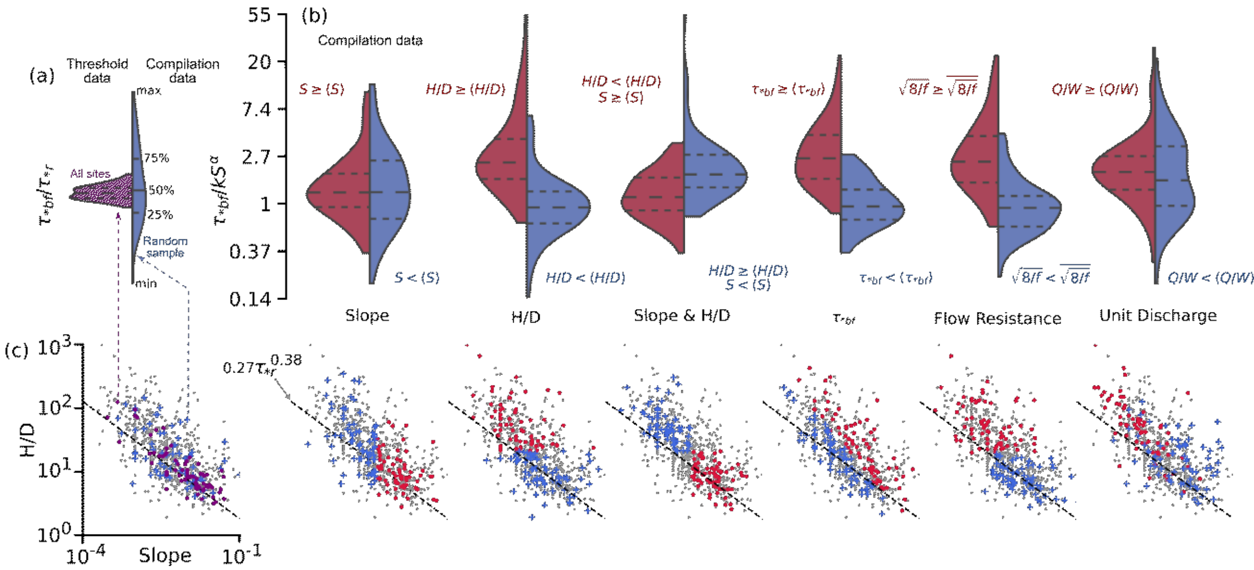

Figure 5. Illustration of bias in estimating transport capacity for various sampling strategies using equation (4). (a) Split violin showing the measured transport capacity for the threshold field sites (purple, n=68, identical to Figure 1b) and a random sample (blue, n=70) from the compilation dataset where the transport capacity is calculated via equation (4). (a) and (b) share the same vertical axis. (b) Transport capacity calculated via equation (4) for various data sampling strategies from the compilation data. Each column represents sampling the larger compilation based on the variable listed below and each half represents 70 randomly selected field sites for the adjacently labeled condition. All data except flow resistance are natural log transformed prior to computing the distributions. (c) Illustration of the random samples used to compute the distributions in (a) and (b) from the larger compilation (small gray dots). All columns in (c) share the same axes. Blue crosses correspond to the right half and red dots represent the left half of the split violins in (b) directly above each data cloud. The black dashed line is equation (3). Note the distributions illustrate how one can observe a potential difference in transport capacity between gravel-bedded rivers based on how the samples relate to equation (3). The observed difference is spurious due to the selection variable's underlying correlation with slope.